

Supporting Information

Structural Evolution and Lithium-Storage Mechanism of the FeTiO₃@Fe₂TiO₅ Endogenous Heterojunction

Yang Chen^a, Ye Li^a, Xiaohuan Wang^{a*}, Huijun Kang^b, Zhiming Shi^a, Guojun Ji^c, Zhipeng Yuan^a

^a School of Materials Science and Engineering, Inner Mongolia University of Technology, Hohhot, 010051, China

^b Key Laboratory of Solidification Control and Digital Preparation Technology (Liaoning Province), School of Materials Science and Engineering, Dalian University of Technology, Dalian, 116024, China.

^c School of Chemical Engineering, Inner Mongolia University of Technology, Hohhot, 010051, China

*Corresponding author: wangxiaohuan@imut.edu.cn (X. Wang)

Calculation formula:

Different scan rates ranging from 0.1 to 1.0 mV s⁻¹ were used for CV testing (**Figure 3f**). The peak current (*i*) follows equations (1) and (2) with respect to the scan rate (*v*):

$$i = av^b \quad (1)$$

$$\log(i) = b \log(v) + \log(a) \quad (2)$$

Where *i* represents the peak current during measurement, while *a* and *b* are constants. The value of *b* is the slope in equation (2). The value of *b* close to 0.5 indicates diffusion-controlled process, while *b* close to 1.0 represents pseudocapacitive process¹. The contributions of pseudocapacitance and ion diffusion control are calculated using equations (3) and (4):

$$i = k_1v + k_2v^{1/2} \quad (3)$$

$$i/v^{1/2} = k_1v^{1/2} + k_2 \quad (4)$$

Where *k*₁ and *k*₂ are constants, *k*₁*v* is related to the surface pseudo-capacitance, and *k*₂*v*^{1/2} is related to the diffusion process^{2,3}

Utilizing the Galvanostatic Intermittent Titration Technique (GITT) to unveil the rate of lithium-ion diffusion, the lithium-ion diffusion coefficient (*D*_{Li}) is measured under a current of 100 mA within the voltage range of 0.01 to 3 V. The calculation formula (5) is as follows:

$$D = \frac{4}{\pi\tau} \left(\frac{m_B V_M}{M_B S} \right)^2 \left(\frac{\Delta E_S}{\Delta E_\tau} \right)^2 \quad (5)$$

Where τ represents the relaxation time, m_B stands for the electrode specific mass, V_M is the molar volume, M_B denotes the molar weight of the electrode, S represents the surface area of the electrode, ΔE_S denotes the steady-state potential change caused by the current pulse, and ΔE_τ refers to the voltage variation during the discharge pulse process⁴.

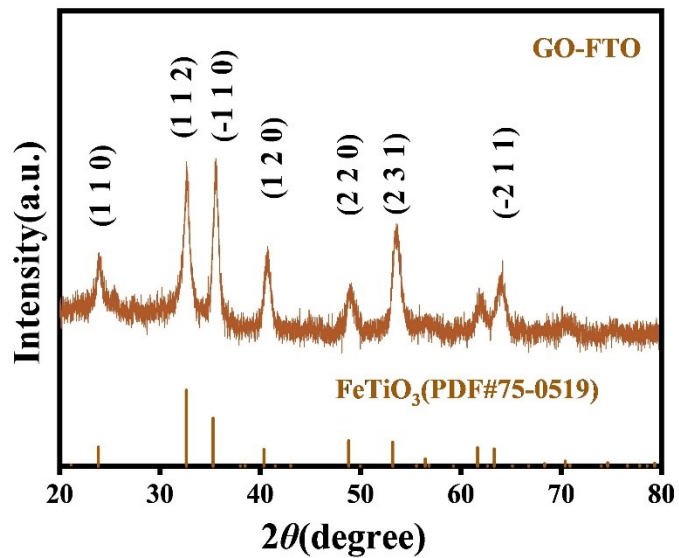


Figure S1 XRD pattern of GO-FTO

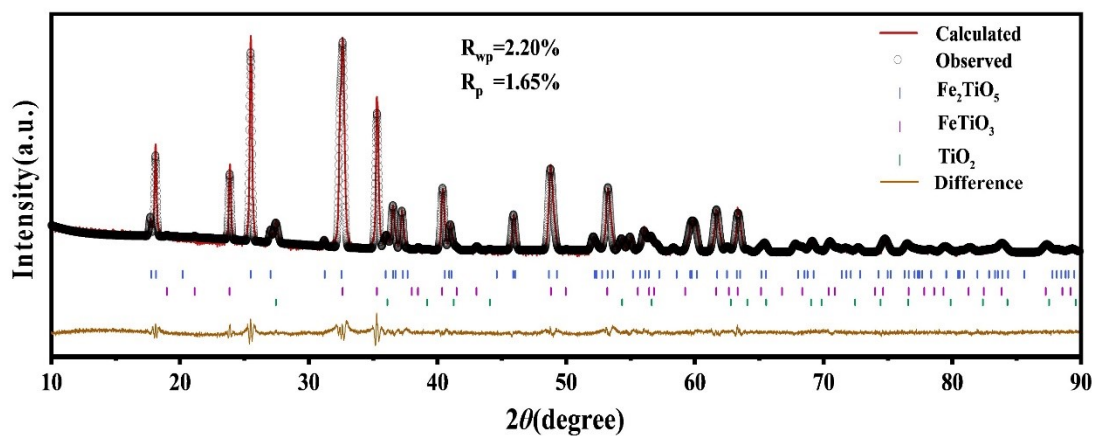


Figure S2 X-ray diffraction patterns and fitting results of hetero-FTO.

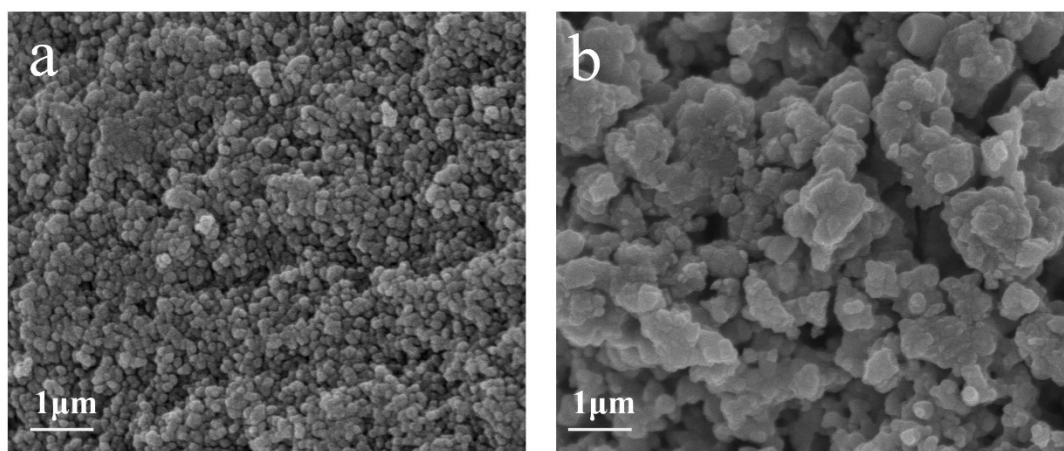


Figure S3 SEM images of FTO(a) and hetero-FTO(b).

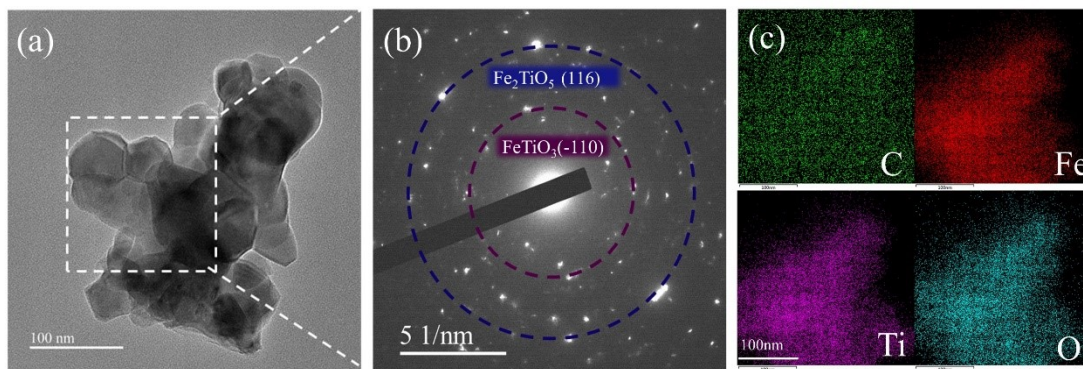


Figure S4 (a)TEM image. (b) SAED. (c) TEM elemental mapping of hetero-FTO.

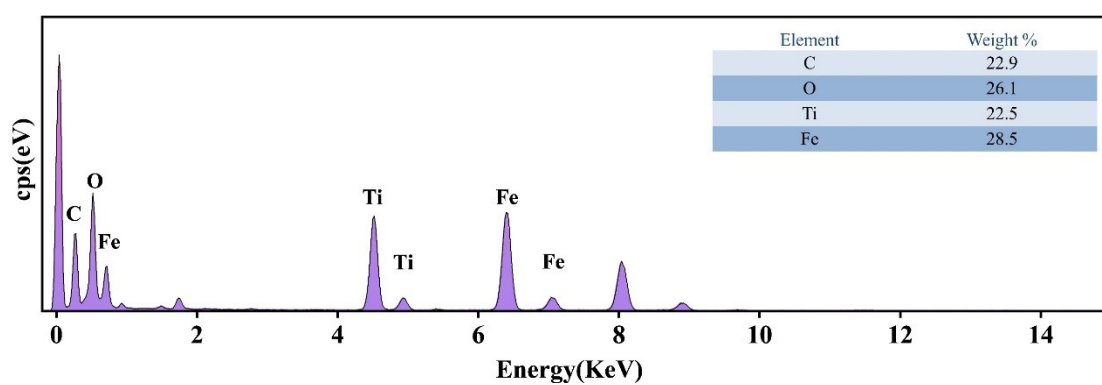


Figure S5 Corresponding EDS spectrum of the area marked.

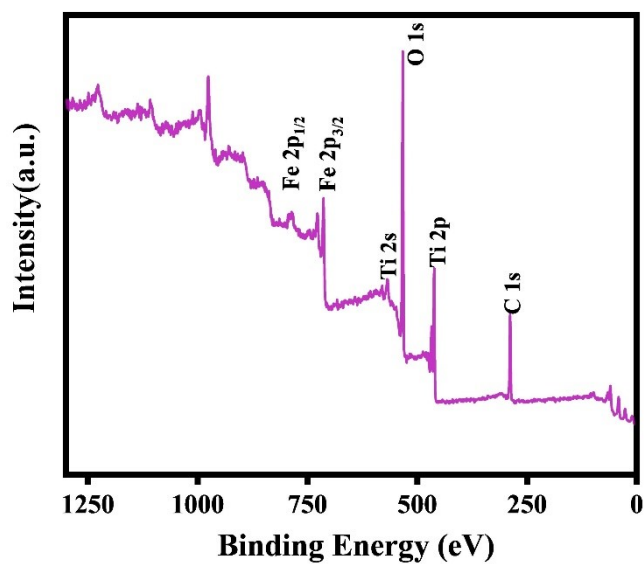


Figure S6 XPS survey spectrum of hetero-FTO.

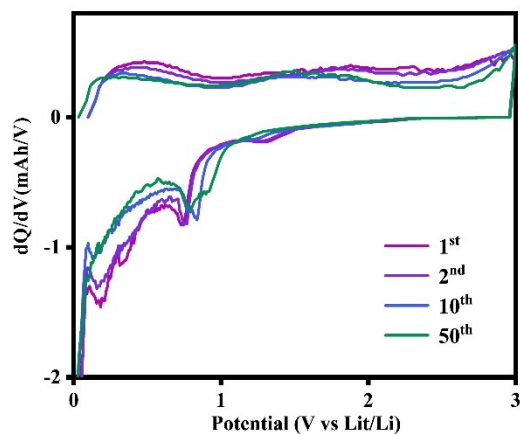


Figure S7 dQ/dV curve.

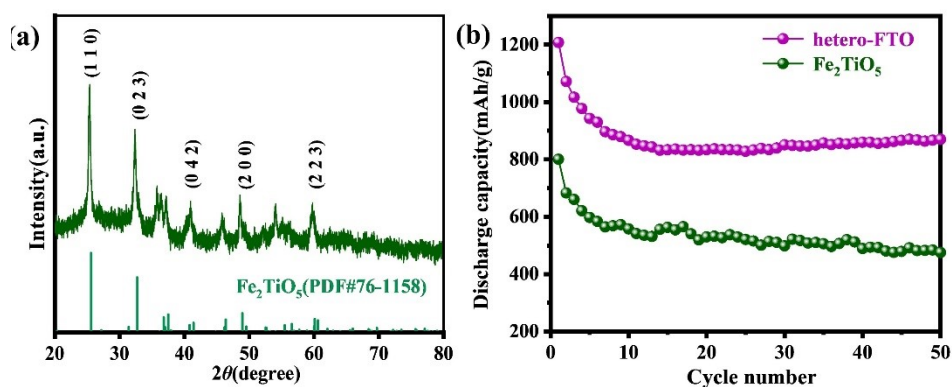


Figure S8 (a) XRD pattern of Fe_2TiO_5 , (b) Cycling performance of Fe_2TiO_5 and hetero-FTO at 100 mA g^{-1} .

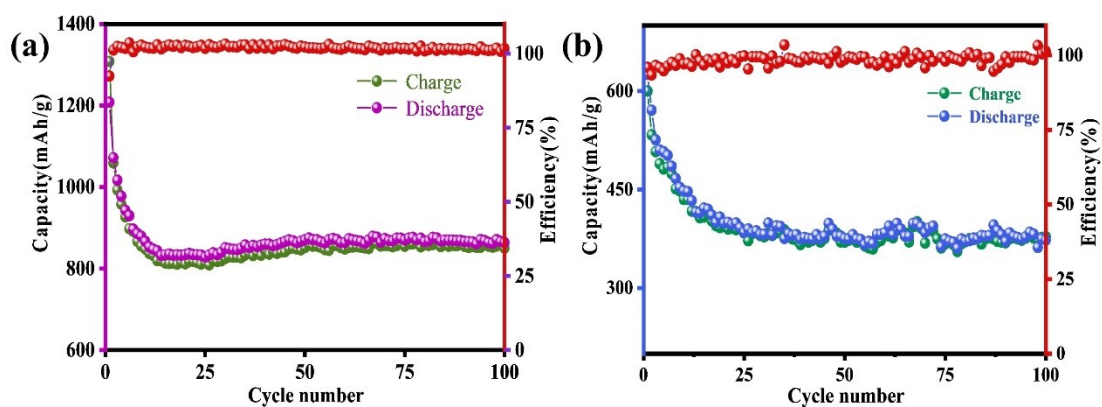


Figure S9 Cyclic Coulomb efficiency diagram of hetero-FTO (a) and FTO (b).

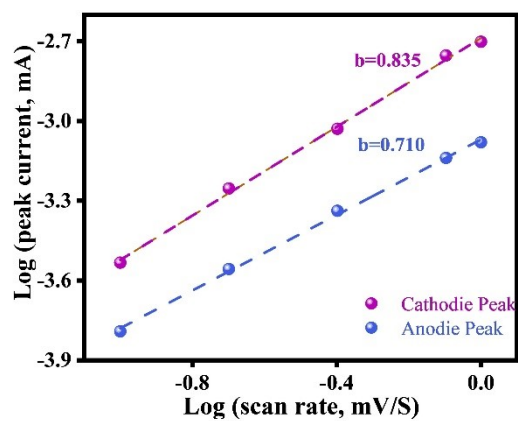


Figure S10 Calculated b value by CV.

Table 1. Calculation of impedance value by EIS

Sample	R_e	R_{sf}	R_{ct}
FTO	1.052 Ω	59 Ω	123.8 Ω
hetero-FTO	1.683 Ω	2.84 Ω	71.37 Ω

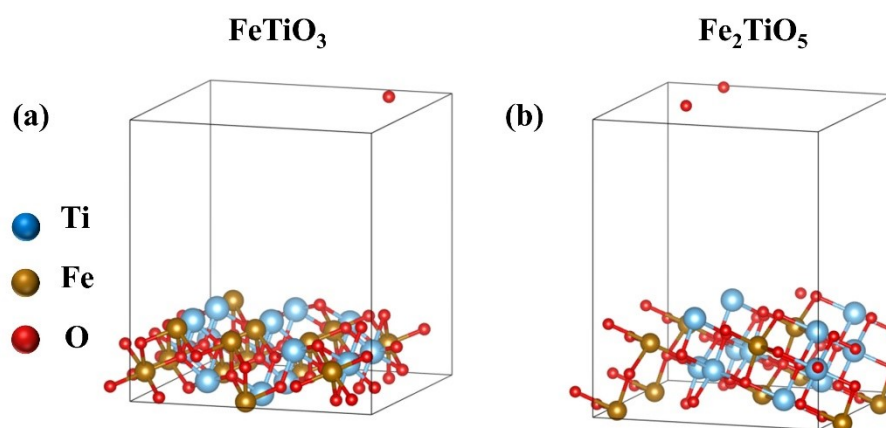


Figure S11 DFT calculation side views (a) $\text{FeTiO}_3(1\ 2\ 0)$. (b) $\text{Fe}_2\text{TiO}_5(1\ 1\ 3)$.

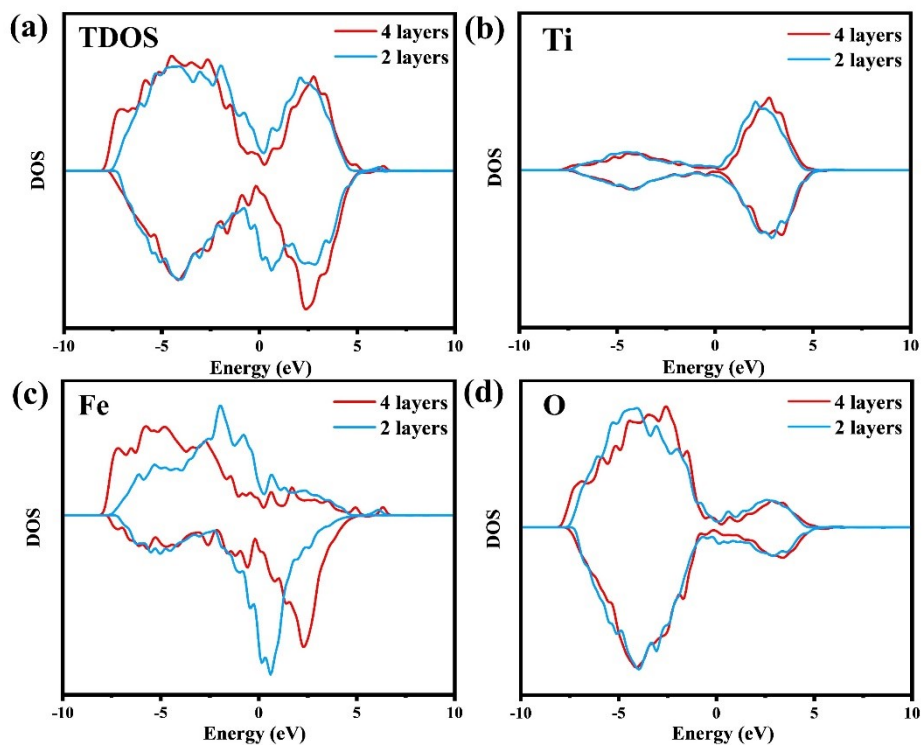


Figure S12 Comparative analysis of the DOS for the $\text{FeTiO}_3@Fe_2TiO_5$ heterojunction in the 2 layers model and 4 layers model.

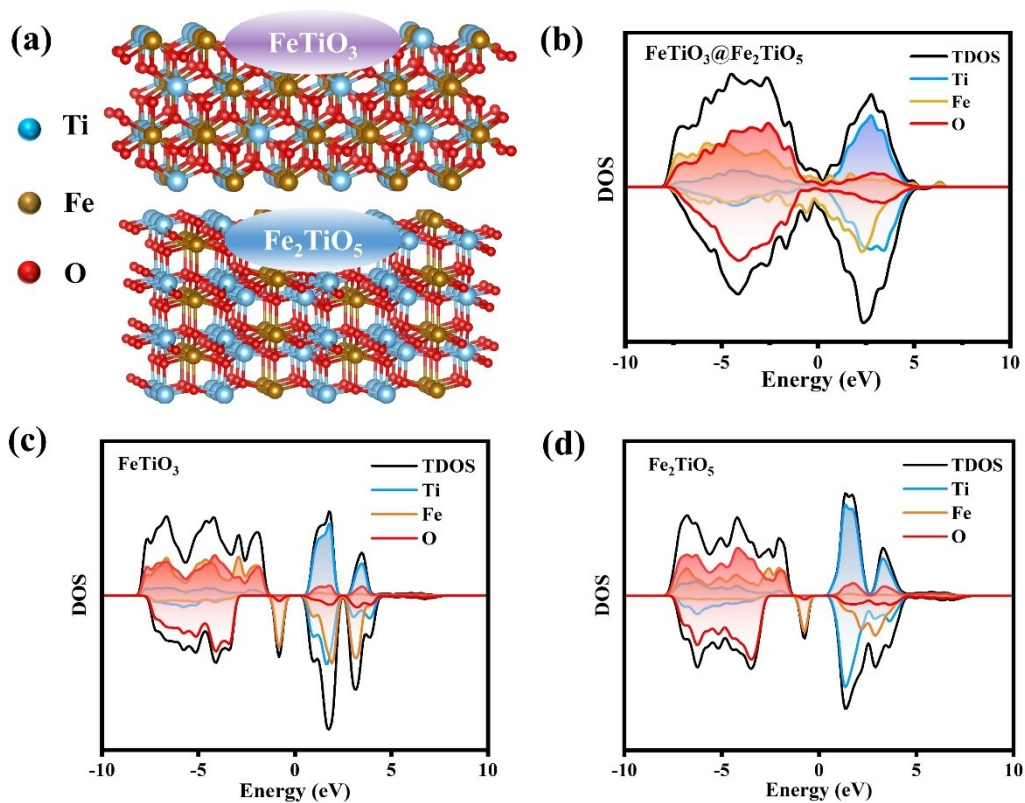


Figure S13 (a) Side-view of the $\text{FeTiO}_3@Fe_2TiO_5$ heterojunction. (b-d) DOS calculation of $\text{FeTiO}_3@Fe_2TiO_5$ heterojunction, FeTiO_3 and Fe_2TiO_5 in 4 layers structural model.

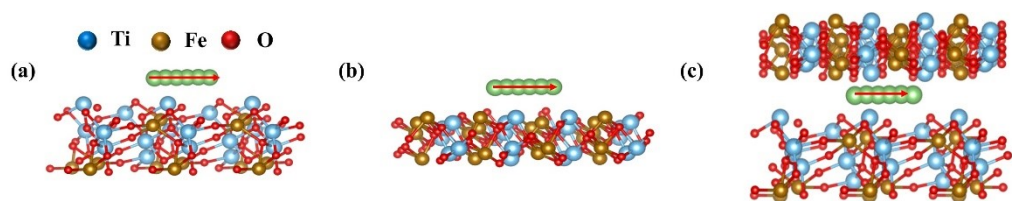


Figure S14 The diffusion of lithium-ions (a) surface of Fe_2TiO_5 , (b) surface of FeTiO_3 , (c) heterojunction interface of $\text{FeTiO}_3@ \text{Fe}_2\text{TiO}_5$.

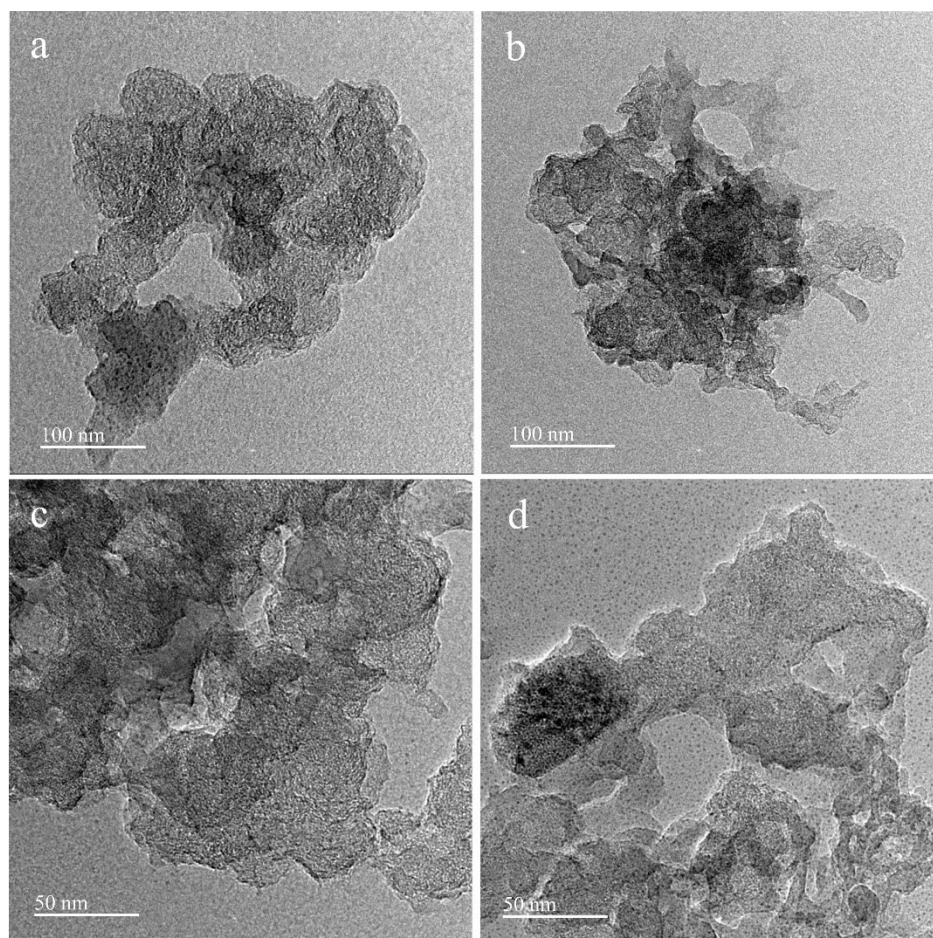


Figure S15 (a) TEM image of the first discharge cycle. (b) the first charge cycle. (c) the 50th charge cycle and (d) the 100th charge cycle.

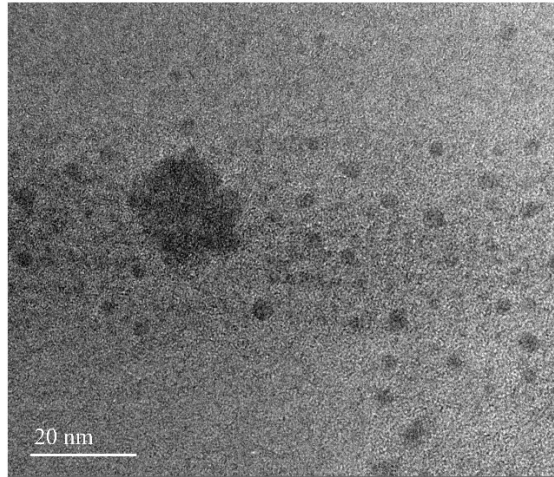


Figure S16 TEM image of the 100th charge cycle.

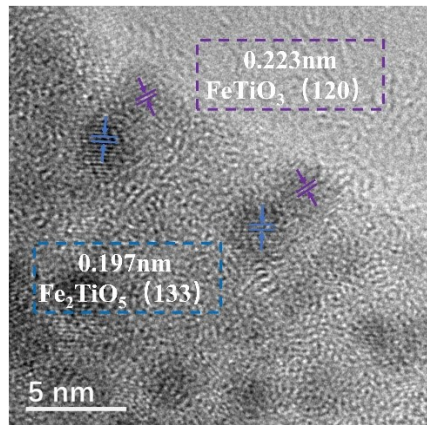


Figure S17 HRTEM of the first charge cycle.

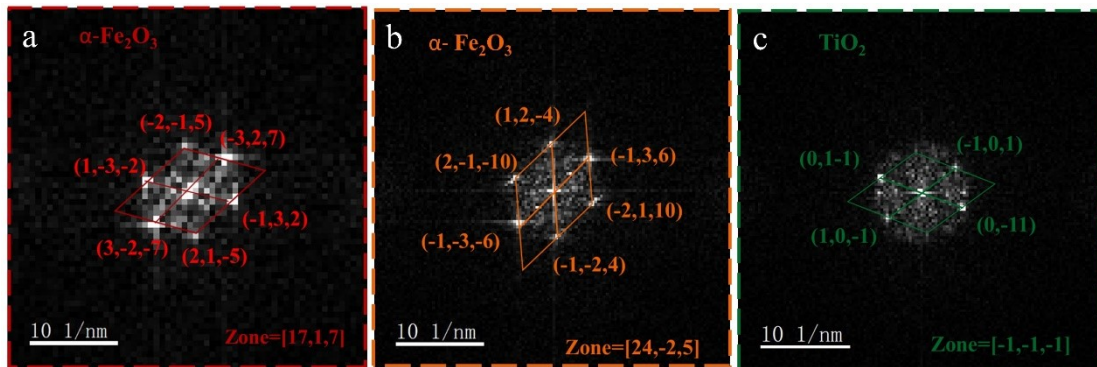


Figure S18 FFT of 50th charge (Fig.6d).

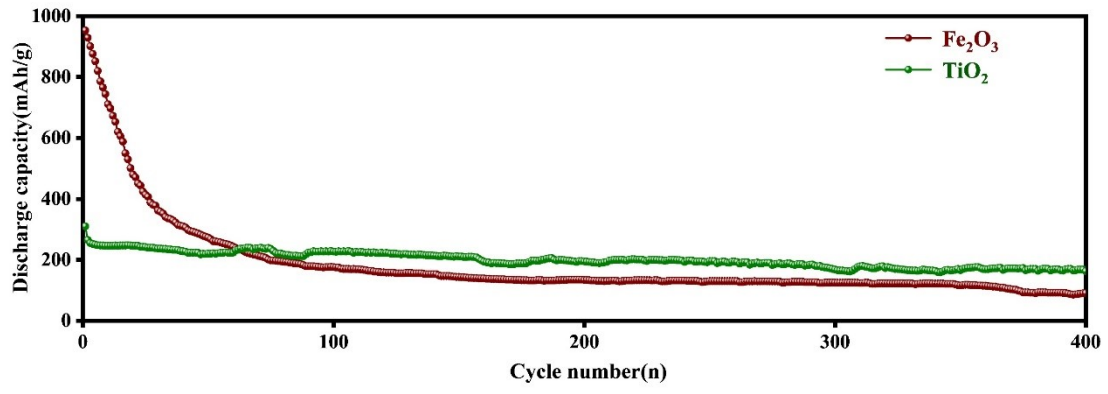


Figure S19 Cycling performance of Fe₂O₃ and TiO₂ at 100 mA g⁻¹

1. Chen, Y.; Chen, H. Y.; Du, F. H.; Shen, X. P.; Ji, Z. Y.; Zhou, H. B.; Yuan, A. H., In-situ construction of nano-sized Ni-NiO-MoO₂ heterostructures on holey reduced graphene oxide nanosheets as high-capacity lithium-ion battery anodes. *J. Alloys Compd.* **2022**, *926*, 166847.
2. Guo, S. S.; Koketsu, T.; Hu, Z. W.; Zhou, J.; Kuo, C. Y.; Lin, H. J.; Chen, C. T.; Strasser, P.; Sui, L. J.; Xie, Y.; Ma, J. W., Mo-Incorporated Magnetite Fe₃O₄ Featuring Cationic Vacancies Enabling Fast Lithium Intercalation for Batteries. *Small* **2022**, *18* (40), 2203835.
3. Ma, L. L.; Zhou, X. M.; Sun, J.; Zhang, P.; Hou, B. X.; Zhang, S. H.; Shang, N. Z.; Song, J. J.; Ye, H. J.; Shao, H.; Tang, Y. F.; Zhao, X. X., Synergy mechanism of defect engineering in MoS₂/FeS₂/C heterostructure for high-performance sodium-ion battery. *J. Energy Chem.* **2023**, *82*, 268-276.
4. Zhang, S. Q.; Sun, L. L.; Yu, L.; Zhai, G. H.; Li, L. X.; Liu, X. J.; Wang, H., Core-Shell CoSe₂/WSe₂ Heterostructures@Carbon in Porous Carbon Nanosheets as Advanced Anode for Sodium Ion Batteries. *Small* **2021**, *17* (49), 2103005.